Applied Physics Letters

Insight on hydrogen injection and GdO_x/Co interface chemistry from *in operando* neutron reflectometry and secondary ion mass spectrometry

Cite as: Appl. Phys. Lett. **122**, 022407 (2023); https://doi.org/10.1063/5.0128835
Submitted: 30 September 2022 • Accepted: 29 December 2022 • Published Online: 13 January 2023

S. Sheffels, P. P. Balakrishnan, M. Huang, et al.

Applied Physics Letters ARTICLE scitation.org/journal/apl

Insight on hydrogen injection and GdO_x/Co interface chemistry from *in operando* neutron reflectometry and secondary ion mass spectrometry

Cite as: Appl. Phys. Lett. **122**, 022407 (2023); doi: 10.1063/5.0128835
Submitted: 30 September 2022 · Accepted: 29 December 2022 ·
Published Online: 13 January 2023

S. Sheffels,[1] P. P. Balakrishnan,[2] M. Huang,[1] S. Muramoto,[3] J. A. Borchers,[2] J. A. Dura,[2] A. J. Grutter,[2] and G. S. D. Beach[1,a)]

AFFILIATIONS

[1]Department of Materials Science and Engineering, Massachusetts Institute of Technology, 77 Massachusetts Avenue, Cambridge, Massachusetts 02139, USA
[2]NIST Center for Neutron Research, National Institute of Standards and Technology, 100 Bureau Drive, Gaithersburg, Maryland 20899, USA
[3]Material Measurement Laboratory, National Institute of Standards and Technology, 100 Bureau Drive, Gaithersburg, Maryland 20899, USA

Note: This paper is part of the APL Special Collection on Magneto-ionic and electrostatic gating of magnetism: Phenomena and devices.
[a)]**Author to whom correspondence should be addressed:** gbeach@mit.edu

ABSTRACT

Ionic and redox control of magnetism can produce large changes to a variety of magnetic properties using a relatively small voltage. A model structure that continues to be of interest is Pt/Co/GdO_xH_y/Au, where the Co magnetic layer oxidation state and perpendicular magnetic anisotropy can be toggled using voltage control of proton transport through the GdO_xH_y electrolyte layer. The hydration of the oxide layer to form a hydroxide phase is the key to improve the speed of these magneto-ionic devices, but there is insufficient understanding of protonic defect incorporation and transport during hydration and electrical gating. In this work, we use polarized neutron reflectometry (PNR) to observe the effects of hydration and electrical gating by scanning in an as-grown state, a hydrated state, and *in operando* during electrical gating. We directly measure the depth profile of hydrogen and confirm the transformation from oxide (Gd_2O_3) to hydroxide [$Gd(OH)_3$]. We observe the accumulation of H in the Co magnetic layer and the effects of gating on the structure and hydrogen content of the other layers in the device stack. Using PNR and secondary ion mass spectrometry, we find evidence for much more complex chemistry at the Co/GdO_xH_y interface than was previously assumed, including evidence for persistent CoO phases and CoO_xH_y phases. We offer insight on using PNR to observe relatively fast proton dynamics in the system and fitting a rather complex set of parameters to achieve a physical result for the fit spectrum and scattering length density profiles.

Voltage control of magnetic films and interfaces using ionic transport or magnetoionics[1,2] introduces the possibility of inducing large changes in magnetic properties using straightforward low-voltage gating. Magneto-ionic mechanisms have the potential to dramatically improve the energy efficiency of magnetic memories and spintronic devices.[3] A variety of ions have been used, most notably oxygen,[1,2,4,5] lithium,[6] hydrogen,[5,7–9] and nitrogen,[10] and large changes in properties, such as magnetic anisotropy,[2,7,11,12] magnetization,[2,5,6,11–13] exchange bias,[4,14] spin–orbit torque,[15,16] and control of magnetic textures,[17,18] have been observed. Pt/Co/oxide stacks are common magneto-ionic devices, where Co is the ferromagnetic layer, Pt provides the spin–orbit coupling needed to give the Co film perpendicular magnetic anisotropy (PMA), and the oxide is the ionic conductor and reservoir and also contributes to interfacial PMA through

Co–O bonding.[19] Originally, oxygen ion migration alone was assumed to cause ionically induced changes in Co/GdO_x. Previous works illuminate hydrogen's role in the redox chemistry of these devices and establish room temperature proton conduction as a mechanism for modulating the Co magnetism.[7,8] Other works have highlighted the importance of humidity and protonic defects in memristors and magneto-ionic devices.[20–24]

Protonic defects ($OH_O^{\bullet}$) are created through the following reaction (given in Kroger–Vink notation) when oxides absorb water from the atmosphere:[25–27]

$$H_2O + O_O^x + V_O^{\bullet\bullet} \rightarrow 2OH_O^{\bullet}. \quad (1)$$

Protons in oxides typically conduct through the Grotthuss mechanism, which consists of two steps: proton reorientation around the oxide ion and hopping to the next oxygen site.[26] Protonic defects are especially important in rare earth oxides, which are very hygroscopic[28] and react with water to form hydroxides such as $Gd(OH)_3$.[29] This phase transition has been shown to change ionic[30] and electrical[29] properties.

Prior works show that positively gating a Pt/Co/GdO_x/Au stack (the Au electrode adjacent to air at high potential) splits water from the ambient water vapor and pumps protons into GdO_x. The electric field drives protons to the Co/GdO_x interface, interrupting the interfacial PMA and causing a reversible magnetic reorientation transition (MRT) to an in-plane state.[7] In devices with an initially oxidized Co layer (CoO), pumping in hydrogen reduces CoO to Co.[7,8] The reverse process happens under negative bias with H_2O oxidizing Co.[7] Previous works used x-ray reflectivity (XRR) to show that during hydration of a GdO_x film in a humid environment, a layer of $Gd(OH)_3$ grows from the surface, and without this hydration step, the device does not function.[8] Other works have used x-ray and neutron reflectivity to show similar protonated surface layers in proton-conducting oxide films (e.g., In-doped $BaZrO_3$).[31] However, x-ray probes are relatively insensitive to hydrogen and instead probe changes in the electron density (primarily the Gd density). Unlike other elements in the system, hydrogen has a negative neutron scattering length, so significant protonation sharply suppresses the neutron scattering length density (SLD). Polarized neutron reflectometry (PNR) is also sensitive to the in-plane net magnetization depth profile. PNR is, therefore, an ideal way to examine hydrogen movement and magnetization changes. We first measured the hydrogen depth profile in a GdO_x film using unpolarized neutron reflectometry (NR) and then used PNR to probe the hydrogen depth profile and the magnetism in the Pt/Co/GdO_x/Au stack during *in operando* positive biasing. We verified the results with *ex situ* secondary ion mass spectrometry (SIMS) after positive and negative gating.

First, we investigated the hydration of an unpatterned GdO_x film. A 1 cm^2 GdO_x film was grown on a Si substrate with a thermally grown oxide layer. The film was hydrated at 50 °C and 90% relative humidity for 20 h and was then vacuum annealed at 100, 200, and 250 °C to drive the water out, all while NR scans were performed continuously. Each condition was sustained until no drift occurred between scans (approximately 2 h). After stabilizing at 100 °C, the reflectivity did not return to its initial shape, so we stepped up the temperature until the reflectivity fringes more closely matched the initial value, at which point we assumed most water had been driven out. Figure 1 shows the neutron reflectivities and associated SLD profiles under each condition. Note that throughout this manuscript, error bars and uncertainties represent one standard error. The as-grown GdO_x film thickness is 29.58 ± 0.14 nm, including a 3.94 ± 0.07 nm layer with reduced SLD at the surface, indicating some combination of oxygen deficiency and partial hydration from exposure to ambient humidity. Such surface regions have been seen in proton conducting perovskites.[31] After hydration, the neutron SLD near the air interface decreases further and the thickness of the low-SLD region increases. The hydrated GdO_xlayer is best fit by a bilayer oxide/hydroxide structure with a hydroxide layer thickness of 11.64 ± 0.09 nm for a total

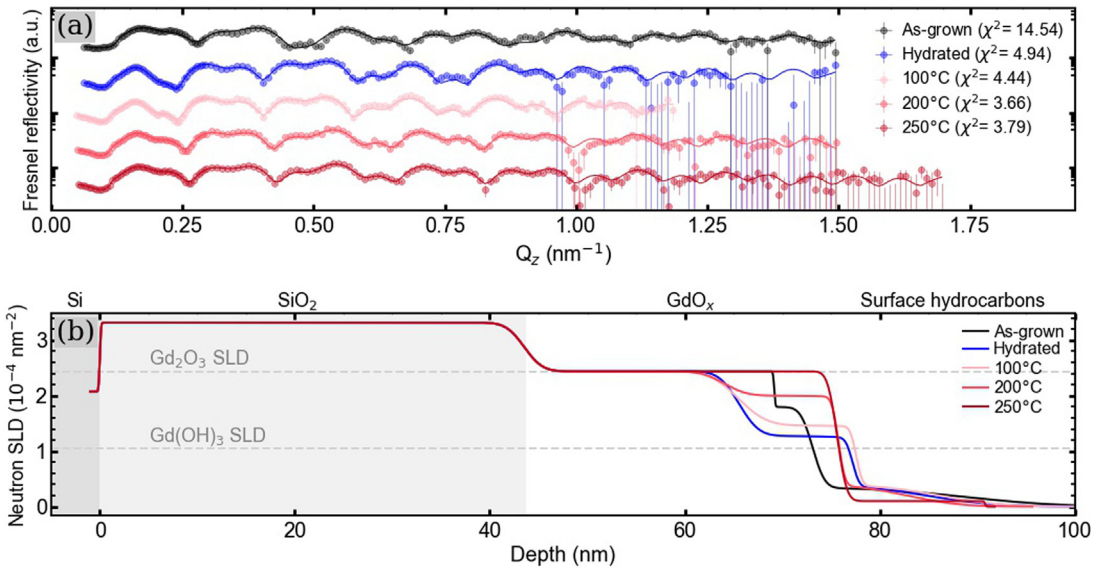

FIG. 1. NR on the unpatterned film showing passive hydration under humid conditions and dehydration upon vacuum annealing. (a) Fresnel reflectivities for as-grown, hydrated 20 h, and vacuum annealed at 100, 200, and 250 °C states. (b) Neutron SLD profiles for the same conditions.

GdO_x thickness of 33.67 ± 0.18 nm. For comparison to a linear gradient fit, see the NR section of the supplementary material and Fig. S1. This bilayer structure confirms that hydration occurs through a phase transition to $Gd(OH)_3$ with a front that extends deeper into the film with longer hydration time (see Fig. S2 for NR reflectivities displaying hydroxide expansion over time). The 13.8% thickness increase during 20-h hydration is consistent with the previously reported 15% thickness increase for 24-h hydration of a similar film measured with XRR.[8]

Several factors simultaneously affect the hydroxide SLD. As the phase transition to $Gd(OH)_3$ occurs, the overall material density decreases from 7.41 (bulk Gd_2O_3) to 6.0 g/cm^3 [previously measured density of $Gd(OH)_3$].[8] Although hydrogen incorporation and lattice expansion during the phase transformation are inherently connected, it is useful to consider their effects on the SLD separately. From the decreased number density of Gd and O atoms in the hydroxide phase alone, we expect an SLD decrease in 19% to a value of 1.98×10^{-4} nm^{-2}. Hydrogen incorporation suppresses the SLD further; SLD values significantly below 1.98×10^{-4} nm^{-2} in the hydrated sample, therefore, argue strongly for increased H concentration. The final hydroxide layer SLD is slightly higher than the expected value of 1.05×10^{-4} nm^{-2} [gray dotted line in Fig. 1(a)], meaning the Gd and O density is higher than that expected (perhaps due to some remaining Gd_2O_3) or the H concentration is lower than that expected for stoichiometric $Gd(OH)_3$.

When vacuum annealed at 100 °C, the hydroxide layer SLD increases as hydrogen is driven out. The film thickness decreases above 200 °C with further reduction in the hydrogen concentration in the hydrated layer. At 250 °C, the GdO_xSLD has returned to the as-grown value. Interestingly, the film thickness remains larger than its original value. The 250 °C state does not have a low-SLD surface layer, meaning that between the as-grown and 250 °C states, H in the surface layer of the as-grown film has been driven out and the oxygen content of that surface layer has increased to match the rest of the film. Oxygen incorporated as the film transforms into a hydroxide [according to Eq. (1)] may not be removed during vacuum annealing. The prior XRR results agree that after 6 days of hydration, the film expanded by 50% and decreased its SLD by 28%, giving a 10% increase in the total integrated x-ray SLD consistent with additional oxidation of the film.[8]

The low SLD tail in each profile above Z = 79 nm is probably due to adsorbed hydrocarbons, which desorb above 200 °C. The 250 °C profile, thus, shows a sharp interface instead of a tail.

We now turn to the Pt/Co/GdO_x/Au patterned devices and examine how hydration and voltage gating affect their structure, hydrogen profile, and magnetism. The Pt/Co/GdO_x/Au devices are susceptible to pinholes; so in order to have a device area large enough for PNR, we used an array of 30 1 mm^2 square crossbar devices (see the sample schematic in Fig. S3). We measured the PNR in the as-grown state, after hydration, and during *in operando* biasing at +3 and +10 V. The bias voltages were held constant, and PNR scans were done continuously until the reflectivities stabilized for the duration of one scan (∼12 h). Figure 2 shows the PNR reflectivities and the SLD profiles for all conditions.

After scanning the as-grown state, the sample was hydrated for 6 days at 90 °C, since previous XRR data found that the thickness change was complete within that time.[8] A saturated K_2SO_4 solution maintained the relative humidity at 95%. Comparing the as-grown and hydrated SLD profiles in Fig. 2(b), we see that the GdO_xlayer becomes approximately 25% thicker with hydration. This change is not as dramatic as was seen in the XRR measurement, which could be explained by the Au electrode preventing hydrogen incorporation. Hydration would then have occurred through lateral diffusion and may have been slower or incomplete. This could also explain the lack of the hydrated layer at the top of the GdO_xfilm, unlike what was observed after hydration of the unpatterned film. Lateral diffusion may play a larger role at the Co/GdO_xinterface, which could explain the decreased GdO_x SLD next to the Co layer in the hydrated state. Alternatively, increased defect concentration near the bottom interface may cause preferential H occupation. The GdO_xSLD starts near the expected bulk value for Gd_2O_3, 2.44×10^{-4} nm^{-2}, and approaches the expected $Gd(OH)_3$ SLD value of 1.05×10^{-4} nm^{-2} after hydration and gating. The low GdO_xSLD near the Co layer after gating is likely due to the low hydrogen solubility in Pt, which makes hydrogen accumulate near the Co interface as it is pumped in. It could also be that a hydroxide layer forms at the bottom of the GdO_xlayer and gets thicker as more H is pumped in.

The oxide-to-hydroxide transformation is corroborated with SIMS, which shows increased signal from GdO_xH_yions after gating compared to the as-grown state (Fig. 3). The SIMS devices were unhydrated with any initial hydrogen in GdO_xcoming from ambient water vapor. The presence of GdO_xH_yonly after gating, therefore, confirms that significant additional hydrogen enters the oxide during positive biasing. The SIMS signal for H_2O decreases with positive bias, likely since H_2O on the surface (and also possibly in the oxide's grain boundaries) is split and incorporated into the hydroxide.

Au exhibits a slight thickness increase and a significant SLD decrease upon hydration, which is consistent with water and hydroxide accumulation on the surface. The Au layer roughens significantly and decreases further in thickness upon gating (corroborated with atomic force microscopy in Fig. S4), which is consistent with Au oxidation[32,33] or surface adsorbates. An alternative interpretation is that GdO_xH_yexpands nonuniformly, causing a roughened interface that spreads Au out in Z, giving an apparently thicker, lower SLD film. The increase in diffuse scattering from the Au electrode after gating can be seen by eye, consistent with the significant increase in roughness in the fit. We note that a significant amount of water or hydrogen adhering to this layer may add apparent roughness unrelated to a change in the structure of the underlying gold. Thus, there is considerable uncertainty regarding the gated Au roughness values presented here.

In the as-grown and hydrated fits, the Co layer SLD is $4.280 \pm 0.017 \times 10^{-4}$ and $4.282 \pm 0.013 \times 10^{-4}$ nm^{-2}, respectively, closely matching that of bulk CoO. Partial or complete Co oxidation is unsurprising, as it was exposed to oxygen during reactive sputtering of GdO_x. Upon gating, the Co layer SLD decreases to $1.44 \pm 0.10 \times 10^{-4}$ nm^{-2}. While we expect both reduction of CoO and incorporation of hydrogen to decrease the Co layer SLD, the optimized value is significantly below the bulk Co value of 2.27×10^{-4} nm^{-2}, which is consistent with significant hydrogenation. For additional context, we calculate that the bulk SLD of cobalt hydroxide [$Co(OH)_2$] is 1.54×10^{-4} nm^{-2} while the optimized values for the +3 and +10 V gated conditions are $1.44 \pm 0.10 \times 10^{-4}$ nm^{-2} and $1.111 \pm 0.071 \times 10^{-4}$ nm^{-2}, respectively. Co reduction under positive bias was previously reported in this system, and H incorporation is what depressed the SLD of the surrounding GdO_x, so both processes likely contributed in reducing the Co layer SLD. Increased porosity in Co upon reduction

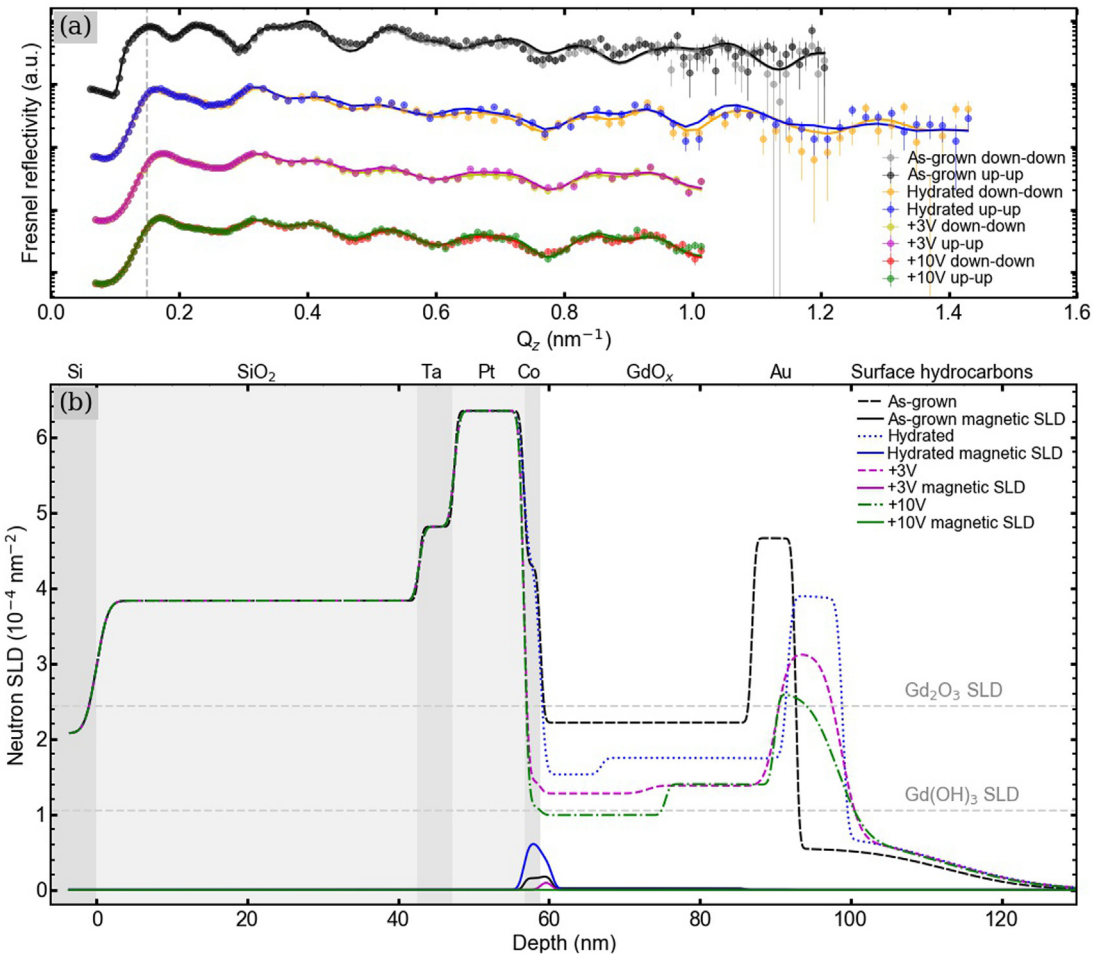

FIG. 2. PNR data for the patterned device in as-grown, hydrated, +3 V gated, and +10 V gated states. (a) Non-spin-flip (↑↑ and ↓↓) Fresnel reflectivities for all four conditions, measured in an applied field of 700 mT. (b) Best fit SLD profiles from the reflectivity data in (a). Both real nuclear and magnetic SLDs are plotted. See the "PNR data reduction and fitting" section in the supplementary material for fitting details.

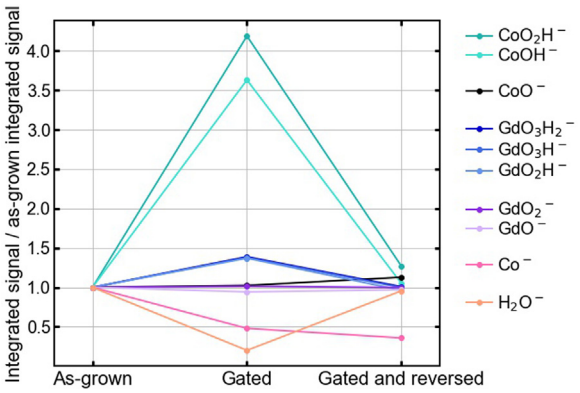

FIG. 3. Integrated SIMS signal for CoO_xH_y, GdO_xH_y, Co, and H_2O ions, measured on three different unhydrated 1 mm^2 crossbar devices gated into different states. See the supplementary material for further information about SIMS measurements.

could also explain the lowered SLD. However, the SIMS data in Fig. 3 show a small Co^- signal that decreases upon gating by 61%, while the $COOH^-$ and $COOH_2^-$ signals increase by 217% and 328%, respectively. Furthermore, while SIMS confirms the presence of CoO compounds in the device, the gating does not result in a significant change in the integrated CoO intensity. Instead, the largest variations in the SIMS intensity are confined to hydrogen-containing species, supporting hydration as the major cause of SLD reduction over increased porosity, although likely both play a role. Note that we looked extensively in the SIMS data for evidence of cobalt hydrides (CoH_x) and found none. CoH_x compounds form only at extremely high pressure, so while we see evidence of H in the Co layer, a CoH_x phase is unlikely.[34]

We found several unexpected results in the magnetic portion of the PNR and in the SIMS data, which lead us to a more complex model of the chemistry of the Co magnetic layer. Our first unexpected finding is that in all states, as-grown, hydrated, and gated, the Co layer had much smaller magnetic SLD than expected—only 15% the bulk

Co value of 1400 emu/cm^3 (1 emu/cm^3 = 1 kA/m), which corresponds to an expected magnetic SLD of 4.12×10^{-4} nm^{-2}. An in-plane field of 700 mT was applied to pull the Co magnetization in-plane, so any magnetization should be visible in the magnetic SLD profile [Fig. 2(b)]. One possible explanation is that only a few devices contained unoxidized Co. However, constraining the fit to have a very small "active device" area with metallic ferromagnetic Co worsens the fit significantly, so this is not likely. Enough Co was present in all as-grown devices to measure a polar MOKE signal displaying PMA (see Fig. S5). Thus, in the as-grown state, the diminished Co magnetization can be explained by a mixed phase of CoO and Co in accordance with the structural analysis.

The second unexpected result is that the Co magnetization grows after hydration and decreases during biasing. To understand why the magnetic SLD is fit this way, we examine the Fresnel spin difference, or the difference of the non-spin-flip reflectivities (↑↑ minus ↓↓), normalized by the theoretical reflectivity of the bare Si substrate. Figure 2(a) shows the spin-dependent neutron reflectivities for the four measurement conditions, and Fig. 4 shows the Fresnel difference of those reflectivities. Figures 4(b)–4(e) show detailed views of the low-q regions. The amplitude of the oscillations in the Fresnel difference is proportional to the total magnetization in the film. The Fresnel difference oscillates in all conditions, and for the first four (lowest q) peaks, the amplitude of the oscillation in the positive biased state is smaller than the amplitude in the hydrated state, implying that the hydrated state must have a larger magnetic SLD than the as-grown and biased states. Figure S6 gives the statistical analysis of these data. Based on previously reported MOKE measurements, we would expect CoO to be reduced to Co with the presence of H_2O under positive bias, which (absent any other chemical or structural changes) should increase the net magnetization. It is possible that some CoO is in fact reduced, but that other effects, discussed below, obscure the effect on the measured magnetization.

The third unexpected result is that the Fresnel spin difference below the critical edge ($Q_{crit} = 0.1$ nm^{-1}) is nonzero [shown clearly in Fig. S6(a)], indicating that some magnetization is co-located with a neutron absorber (Gd) in the film. Co and GdO_x were thought to be distinct layers, while GdO_x itself is not magnetic. The best description of this feature appears when a layer of GdO_x near the Co/GdO_x interface is allowed to express a net magnetization in the model. This interfacial magnetization is notably reduced upon gating. One explanation for magnetized Gd is an intermixed sublayer of Co and GdO_x (possibly also including Pt). Paramagnetic behavior in Co-doped nanocrystalline GdO_x at room temperature has been observed.[35] The intermixing could have occurred during sputtering, which is common especially for heavy elements,[36] or possibly during hydration, when the sample was held at 90 °C for 6 days. Intermixing can explain the suppression of Co magnetization below the bulk value in the as-grown and hydrated states, especially if the Co and Gd develop antiparallel moments. It could similarly explain the increase in magnetization upon hydration and the suppression during gating. If indeed Co and Gd intermixing suppresses magnetization in the as-grown state, deconvoluting the chemistry controlling the net moment becomes nontrivial with Co and Gd reacting with O and H in ways which may have offsetting effects.

The SIMS results lend credence to this picture. The SIMS shows that CoO_xH_y ions are present and the total signal from $CoOH^-$ and $CoOH_2^-$ increases after positive gating and decreases back to initial values upon negative gating. These results imply that some oxygen remains in the Co layer (or an intermixed layer) and the hydrogen driven in during positive gating penetrates this layer and forms a cobalt hydroxide phase. We conclude that the model of toggling between completely metallic and completely oxidized states is not accurate. In reality, CoO, Co, and CoO_xH_y phases may co-exist with the relative prevalence of each phase changing under different hydration and gating conditions. These complexities would not be observable in MOKE measurements, which primarily probe the metallic Co. The Pt/Co/GdO_x/Au devices in which CoO/Co toggling was previously measured using MOKE[7,8] may or may not have displayed Pt,

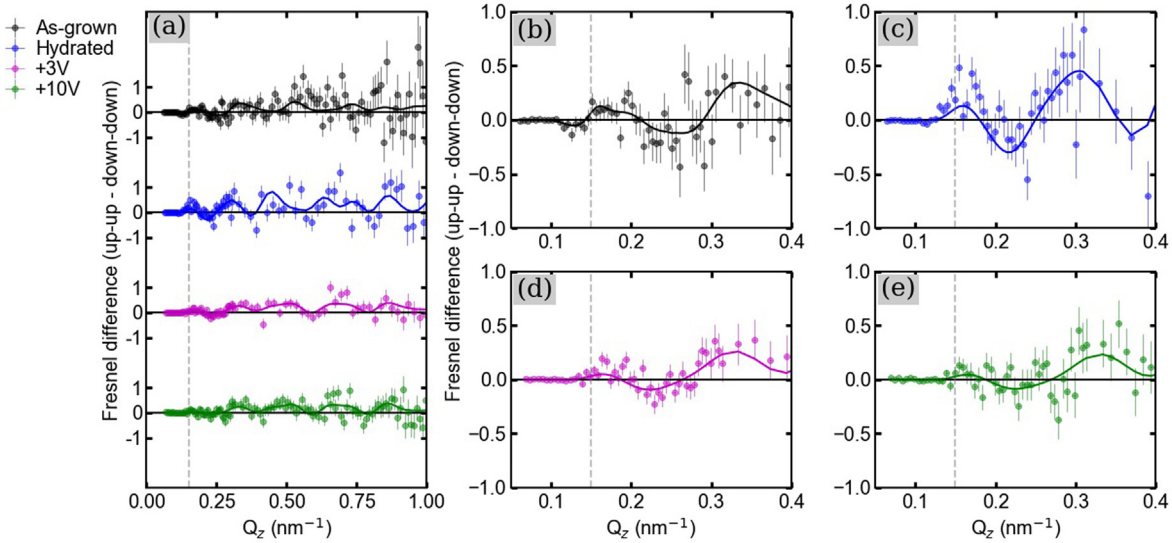

FIG. 4. (a) PNR Fresnel spin difference (↑↑ minus ↓↓) for the patterned sample, calculated from data in Fig. 2(a). (b)–(e) Enlarged views ($Q_z = 0$–0.4) of the first four oscillations for each condition.

Co, and Gd intermixing and mixed Co, CoO, and CoO_xH_y phases. As long as some metallic Co was present, MOKE could still show transitions between a CoO/CoO_xH_y nonmagnetic state and magnetic states containing metallic Co.

The best fit also includes slight paramagnetism in the rest of Gd, including regions that are not next to Co, for all conditions. The hydrated condition has the highest fit value, 1.82 ± 1.19 emu/cm^3. GdO_xnanoparticles have been shown to be paramagnetic at room temperature, so slight paramagnetism in the nanocrystalline GdO_xfilm is reasonable.[37]

We set out to investigate the effects of hydration and voltage gating on the structure and magnetization of the $Pt/Co/GdO_xH_y/Au$ system. The structural PNR results showing depressed SLD due to hydrogen and the SIMS result showing signal from GdO_xH_yions are the first direct measurements of hydrogen in this system; along with the NR results, they support the models for phase transformation from oxide to hydroxide during hydration of $GdO_x$and for water splitting and proton incorporation during positive biasing. NR results show an increase in the total integrated GdO_xlayer SLD after hydration and vacuum annealing, which we attribute to irreversible uptake of oxygen. During voltage gating, H accumulates in the Co layer and in the GdO_xlayer near the Co/GdO_xinterface. The hydrogen concentration, the depth of the phase transformation front, and the amount of GdO_xH_ycompounds all increased further with gating, indicating that incomplete hydration can be compensated by adding hydrogen during biasing.

The prevailing model of this system suggested that voltage gating induced complete transformations among a nonmagnetic CoO state, an in-plane Co state with H loaded at the GdO_xH_yinterface, and a PMA Co state with no H loaded. This work complicates that model. The PNR and SIMS results reveal the presence of CoO, CoO_xH_y, and a smaller-than-expected amount of Co as well as a possibly intermixed layer of Pt, Co, and Gd that suppresses the net magnetization. Lower temperatures during hydration or more optimized deposition could reduce intermixing and the evolution of unwanted species. Furthermore, it may be possible to substantially tune the switching behavior and magnetization changes through judicious selection of the initial Co state. A partially oxidized CoO layer, for example, appears to evolve some fraction of Co hydroxide species, while such reactions may be suppressed in completely metallic Co. This work sheds light on the complicated interface chemistry and chemical irreversibility crucial to understand and tune voltage-controlled magneto-ionic devices.

See the supplementary material for figures illustrating the alternate gradient NR fit for the unpatterned film, the expansion of the unpatterned film over time during hydration, a schematic and initial MOKE loop for the sample used for the PNR experiments, a statistical analysis of the Fresnel spin difference of the PNR reflectivities, and the SLD profiles for all nonactive regions on the PNR sample. It also includes the experimental details for all measurements performed in this work, including a detailed discussion of the fitting parameters and constraints used in the PNR analysis of this multi-region, multi-condition system.

This work was supported in part by the U.S. National Science Foundation (NSF) through the Massachusetts Institute of Technology Materials Research Science and Engineering Center (MRSEC) under Award No. DMR-1419807 and through SMART, one of the seven centers of nCORE, a Semiconductor Research Corporation Program, sponsored by the National Institute of Standards and Technology (NIST).

AUTHOR DECLARATIONS

Conflict of Interest

The authors have no conflicts to disclose.

Author Contributions

Sara Sheffels: Conceptualization (equal); Formal analysis (equal); Investigation (equal); Methodology (equal); Visualization (equal); Writing – original draft (equal); Writing – review & editing (equal). **Purnima Parvathy Balakrishnan:** Formal analysis (equal); Investigation (equal); Methodology (equal); Writing – review & editing (equal). **Mantao Huang:** Conceptualization (equal); Investigation (equal); Methodology (equal); Writing – review & editing (equal). **Shin Muramoto:** Formal analysis (equal); Investigation (equal); Methodology (equal); Writing – review & editing (equal). **Julie Ann Borchers:** Formal analysis (equal); Investigation (equal); Methodology (equal); Writing – review & editing (equal). **Joseph A. Dura:** Formal analysis (equal); Investigation (equal); Methodology (equal); Writing – review & editing (equal). **Alexander Grutter:** Conceptualization (equal); Formal analysis (equal); Investigation (equal); Methodology (equal); Writing – original draft (equal); Writing – review & editing (equal). **Geoffrey S. D. Beach:** Conceptualization (equal); Formal analysis (equal); Funding acquisition (equal); Methodology (equal); Writing – review & editing (equal).

DATA AVAILABILITY

The data that support the findings of this study are available from the corresponding author upon reasonable request.

REFERENCES

[1]U. Bauer, S. Emori, and G. S. Beach, "Voltage-controlled domain wall traps in ferromagnetic nanowires," Nat. Nanotechnol. **8**, 411–416 (2013).
[2]U. Bauer, L. Yao, A. J. Tan, P. Agrawal, S. Emori, H. L. Tuller, S. V. Dijken, and G. S. D. Beach, "Magneto-ionic control of interfacial magnetism," Nat. Mater. **14**, 174 (2015).
[3]M. Nichterwitz, S. Honnali, M. Kutuzau, S. Guo, J. Zehner, K. Nielsch, and K. Leistner, "Advances in magneto-ionic materials and perspectives for their application," APL Mater. **9**, 030903 (2021).
[4]D. A. Gilbert, J. Olamit, R. K. Dumas, B. J. Kirby, A. J. Grutter, B. B. Maranville, E. Arenholz, J. A. Borchers, and K. Liu, "Controllable positive exchange bias via redoxdriven oxygen migration," Nat. Commun. **7**, 1–8 (2016).
[5]N. Lu, P. Zhang, Q. Zhang, R. Qiao, Q. He, H. B. Li, Y. Wang, J. Guo, D. Zhang, Z. Duan, Z. Li, M. Wang, S. Yang, M. Yan, E. Arenholz, S. Zhou, W. Yang, L. Gu, C. W. Nan, J. Wu, Y. Tokura, and P. Yu, "Electric-field control of tri-state phase transformation with a selective dual-ion switch," Nature **546**, 124–128 (2017).
[6]S. Dasgupta, B. Das, Q. Li, D. Wang, T. T. Baby, S. Indris, M. Knapp, H. Ehrenberg, K. Fink, R. Kruk, and H. Hahn, "Toward on-and-off magnetism: reversible electro-chemistry to control magnetic phase transitions in spinel ferrites," Adv. Funct. Mater. **26**, 7507–7515 (2016).
[7]A. J. Tan, M. Huang, C. O. Avci, F. Büttner, M. Mann, W. Hu, C. Mazzoli, S. Wilkins, H. L. Tuller, and G. S. Beach, "Magneto-ionic control of magnetism using a solid-state proton pump," Nat. Mater. **18**, 35–41 (2019).

[8]A. J. Tan, M. Huang, S. Sheffels, F. Büttner, S. Kim, A. H. Hunt, I. Waluyo, H. L. Tuller, and G. S. Beach, "Hydration of gadolinium oxide (Gd Ox) and its effect on voltage-induced Co oxidation in a Pt/Co/Gd Ox/Au heterostructure," Phys. Rev. Mater. **3**, 064408 (2019).
[9]K. Y. Lee, S. Jo, A. J. Tan, M. Huang, D. Choi, J. H. Park, H. I. Ji, J. W. Son, J. Chang, G. S. Beach, and S. Woo, "Fast magneto-ionic switching of interface anisotropy using yttria-stabilized zirconia gate oxide," Nano Lett. **20**, 3435–3441 (2020).
[10]J. de Rojas, A. Quintana, A. Lopeandía, J. Salguero, B. Muñiz, F. Ibrahim, M. Chshiev, A. Nicolenco, M. O. Liedke, M. Butterling, A. Wagner, V. Sireus, L. Abad, C. J. Jensen, K. Liu, J. Nogués, J. L. Costa-Krämer, E. Menéndez, and J. Sort, "Voltage-driven motion of nitrogen ions: A new paradigm for magneto-ionics," Nat. Commun. **11**, 5871 (2020).
[11]C. Bi, Y. Liu, T. Newhouse-Illige, M. Xu, M. Rosales, J. W. Freeland, O. Mryasov, S. Zhang, S. G. Te Velthuis, and W. G. Wang, "Reversible control of Co magnetism by voltage-induced oxidation," Phys. Rev. Lett. **113**, 267202 (2014).
[12]G. Hao, N. Noviasky, S. Cao, I. Sabirianov, Y. Yin, C. C. Ilie, E. Kirianov, N. Sharma, A. Sokolov, A. Marshall, X. Xu, and P. A. Dowben, "Some device implications of voltage controlled magnetic anisotropy in Co/Gd_2O_3 thin films through REDOX chemistry," J. Magn. Magn. Mater. **451**, 487–492 (2018).
[13]M. Sakamaki and K. Amemiya, "Observation of an electric field-induced interface redox reaction and magnetic modification in GdOx/Co thin film by means of depth-resolved x-ray absorption spectroscopy," Phys. Chem. Chem. Phys. **20**, 20004–20009 (2018).
[14]J. Zehner, D. Wolf, M. U. Hasan, M. Huang, D. Bono, K. Nielsch, K. Leistner, and G. S. Beach, "Magnetoionic control of perpendicular exchange bias," Phys. Rev. Mater. **5**, L061401 (2021).
[15]S. Emori, U. Bauer, S. Woo, and G. S. Beach, "Large voltage-induced modification of spin-orbit torques in Pt/Co/GdOx," Appl. Phys. Lett. **105**, 222401–222406 (2014).
[16]R. Mishra, F. Mahfouzi, D. Kumar, K. Cai, M. Chen, X. Qiu, N. Kioussis, and H. Yang, "Electric-field control of spin accumulation direction for spin-orbit torques," Nat. Commun. **10**, 248 (2019).
[17]M. Huang, M. U. Hasan, K. Klyukin, D. Zhang, D. Lyu, P. Gargiani, M. Valvidares, S. Sheffels, A. Churikova, F. Büttner, J. Zehner, L. Caretta, K. Y. Lee, J. Chang, J. P. Wang, K. Leistner, B. Yildiz, and G. S. Beach, "Voltage control of ferrimagnetic order and voltage-assisted writing of ferrimagnetic spin textures," Nat. Nanotechnol. **16**, 981–988 (2021).
[18]Y. Chen, A. Nicolenco, P. Molet, A. Mihi, E. Pellicer, J. Sort, Y. Chen, A. Mihi, and E. Pellicer, "Magneto-ionic suppression of magnetic vortices," Sci. Technol. Adv. Mater. **22**, 972–984 (2021).
[19]A. Manchon, C. Ducruet, L. Lombard, S. Auffret, B. Rodmacq, B. Dieny, S. Pizzini, J. Vogel, V. Uhlir, M. Hochstrasser, A. Manchon, C. Ducruet, L. Lombard, S. Auffret, and B. Rodmacq, "Analysis of anisotropy crossover due to oxygen in Pt/Co/MOx trilayer," J Appl. Phys. **104**, 043914 (2008).
[20]T. Tsuruoka, I. Valov, C. Mannequin, T. Hasegawa, R. Waser, and M. Aono, "Humidity effects on the redox reactions and ionic transport in a Cu/Ta_2 O_5/Pt atomic switch structure," Jpn. J. Appl. Phys. **55**, 06GJ09 (2016).
[21]F. Messerschmitt, M. Kubicek, and J. L. Rupp, "How does moisture affect the physical property of memristance for anionic-electronic resistive switching memories?," Adv. Funct. Mater. **25**, 5117–5125 (2015).
[22]F. Messerschmitt, M. Jansen, and J. L. Rupp, "When memristance crosses the path with humidity sensing—About the importance of protons and its opportunities in valence change memristors," Adv. Electron. Mater. **4**, 1800282 (2018).
[23]T. Tsuruoka, K. Terabe, T. Hasegawa, I. Valov, R. Waser, and M. Aono, "Effects of moisture on the switching characteristics of oxide-based, gapless-type atomic switches," Adv. Funct. Mater. **22**, 70–77 (2012).
[24]M. Lübben, S. Wiefels, R. Waser, and I. Valov, "Processes and effects of oxygen and moisture in resistively switching TaO_x and HfO_x," Adv. Electron. Mater. **4**, 1700458 (2018).
[25]T. Norby, M. Widerøe, R. Glöckner, and Y. Larring, "Hydrogen in oxides," Dalton Trans. **2004**, 3012–3018.
[26]K. D. Kreuer, "Proton-conducting oxides," Annu. Rev. Mater. Res. **33**, 333–359 (2003).
[27]H. L. Tuller and S. R. Bishop, "Point defects in oxides: Tailoring materials through defect engineering," Annu. Rev. Mater. Res. **41**, 369–398 (2011).
[28]T. Moeller and H. E. Kremers, "The basicity characteristics of scandium, yttrium, and the rare earth elements," Chem. Rev. **37**, 97–159 (1945).
[29]S. Jeon and H. Hwang, "Effect of hygroscopic nature on the electrical characteristics of lanthanide oxides (Pr_2O_3, Sm_2O_3, Gd_2O_3, and Dy_2O_3)," J. Appl. Phys. **93**, 6393–6395 (2003).
[30]Y. Larring and T. Norby, "Protons in rare earth oxides," Solid State Ionics **77**, 147–151 (1995).
[31]L. Mazzei, M. Wolff, D. Pergolesi, J. A. Dura, L. Börjesson, P. Gutfreund, M. Bettinelli, T. Lippert, and M. Karlsson, "Structure and conductivity of epitaxial thin films of in-doped BaZrO3-based proton conductors," J. Phys. Chem. C **120**, 28415–28422 (2016).
[32]K. Ogura, S. Haruyama, and K. Nagasaki, "The electrochemical oxidation and reduction of gold," J. Electrochem. Soc. **118**, 531 (1971).
[33]T. Miyazaki, R. Hasegawa, H. Yamaguchi, H. Oh-Oka, H. Nagato, I. Amemiya, and S. Uchikoga, "Electrical control of plasmon resonance of gold nanoparticles using electrochemical oxidation," J. Phys. Chem. C **113**, 8484–8490 (2009).
[34]M. Wang, J. Binns, M. E. Donnelly, M. Peña-Alvarez, P. Dalladay-Simpson, and R. T. Howie, "High pressure synthesis and stability of cobalt hydrides," J. Chem. Phys. **148**, 144310 (2018).
[35]B. J. Sarkar, A. Bandyopadhyay, J. Mandal, A. K. Deb, and P. K. Chakrabarti, "Paramagnetic to ferromagnetic phase transition of Co doped Gd_2O_3 prepared by chemical route," J. Alloys Compd. **656**, 339–346 (2016).
[36]F. Letellier, V. Baltz, L. Lechevallier, R. Lardé, J. F. Jacquot, B. Rodmacq, J. M. Le Breton, and B. Dieny, "Effects of sputter-deposition-induced and post-deposition thermally activated intermixing on the exchange bias properties of [Pt/Co] ×3/(Pt)/IrMn films," J. Phys. D: Appl. Phys. **45**, 275001 (2012).
[37]C. C. Huang, T. Y. Liu, C. H. Su, Y. W. Lo, J. H. Chen, and C. S. Yeh, "Superparamagnetic hollow and paramagnetic porous Gd_2O_3 particles," Chem. Mater. **20**, 3840–3848 (2008).